ENO and WENO Schemes with the Exact Conservation Property for One-Dimensional Shallow Water Equations

Senka Vukovic[1] and Luka Sopta

University of Rijeka, 51000 Rijeka, Vukovarska 58, Croatia
E-mail: senka.vukovic@ri.hinet.hr and sopta@rijeka.riteh.hr

In this paper we propose new finit difference numerical schemes for hyperbolic conservation law systems with geometrical source terms. In the development of the new schemes we use the essentially nonoscillatory (ENO) and weighted ENO (WENO) reconstruction, developed by Harten, Osher, Engquist, Chakravarthy, Shu, and Jiang, and the idea of the balancing between the flu gradient and the source term, introduced by Bermùdez and Vázquez. Actually, the new schemes are ENO and WENO schemes with the source term decomposed, i.e., the ENO and WENO reconstruction is applied not only to the flu but to a combination of the flu and the source term. In particular, when new schemes are applied to the shallow water equations the new schemes verify the exact conservation property (C-property). We present the algorithm, the proof of the exact C-property, and numerical results for several test problems. © 2002 Elsevier Science (USA)

Key Words: hyperbolic conservation laws; shallow water equations; ENO and WENO reconstruction; C-property.

1. INTRODUCTION

For the numerical approximation of the source term in hyperbolic conservation laws, there are two main approaches: the splitting and the upwinding. The firs consists of splitting the nonhomogeneous hyperbolic conservation laws system into a homogeneous system with the same flu term and an ordinary differential equations system with the source term on the right-hand side. In the second approach, instead of pointwise evaluation of the source term, the source term is upwinded in the same way as the flu term. Roe [20] showed that upwinding is a better strategy, since linear stability analysis for hyperbolic conservation laws

---

[1] Fax: +385 51 651 490.

with source terms shows that upwinding of the source term gives bigger stability regions then pointwise source term evaluations [3, 20]. However, even if the upwinded approach is chosen, there are still different additional diff culties in the source term modeling.

One possible diff culty with source terms comes from relaxation terms, i.e., where the source terms cause a "relaxation" toward equilibrium. There the source term is stiff in the sense that the time scale introduced by it is small compared with the characteristic speed and some other appropriate length scale. Relaxation schemes developed by Jin and Xin [15] lead to such nonhomogeneous conservation law systems and there are many numerical schemes and convergence results for this type of problem, together with ideas for including the source term in f ux numerical approximations [18].

However, we are concerned with another class of problems, one with a low regularity in the source term. This is typical for geometrical source terms that appear in conservation laws for shallow water f ows, one-dimensional open channel f ows, bed-load sediment transport f ows, nozzle f ows, and so forth. For that class of problems a signif cant result was given by Bermùdez and Vázquez [3]. They used Q-schemes and the idea of source term upwinding, introduced the idea of f ux gradient and source term balancing, and def ned the notion of the conservation property (C-property). Up to now, Hubbard and Garcia-Navarro have extended Q-schemes of Bermùdez and Vázquez to a second-order f ux limited scheme with the source term decomposed [9], LeVeque and co-workers have introduced a quasi-steady wave propagation algorithm [16, 17], Jenny and Müller have modif ed a Rankine–Hugoniot–Riemann solver for the presence of source terms [11], Greenberg and LeRoux have proposed a well-balanced scheme [6], Smolarkiewicz and Margolin have extended MPDATA schemes to systems of equations with arbitrary right-hand sides [24], Botchorishvilli *et al.* have given equilibrium schemes which are a combination of the Engquist–Osher schemes and upwind source terms [4], Jin has constructed a steady-state capturing method combining Godunov or Roe-type upwind with source term balancing [14], Chinnayya and LeRoux have developed a new general Riemann solver for the shallow water equations [5], Zhou *et al.* have used the surface gradient method for the treatment of source terms [26], and so forth.

In this paper we propose a new set of numerical schemes that incorporate the concept of f ux gradient and source term balancing into the essentially nonoscillatory (ENO) and weighted ENO (WENO) schemes. The ENO schemes were created by Harten *et al.* [7, 8], while the WENO reconstruction was introduced by Jiang and Shu [12], as an improvement to the original ENO idea. ENO and WENO schemes combine Runge–Kutta-type time integration with the ENO or WENO reconstruction of the f ux term and they are shock capturing, TVD, and with a high order of accuracy [1, 13, 19, 21–23]. Our schemes can be treated as ENO and WENO extensions for the approach of Bermùdez and Vázquez or as f ux gradient and source term balanced versions of ENO and WENO schemes. Particularly, we use ENO and WENO Roe formulation with entropy f x (ENO-RF, WENO-RF) and ENO and WENO locally Lax–Friedrichs formulation (ENO-LLF, WENO-LLF) for the numerical approximation of the f ux. This choice is based on the fact that in the building blocks [1, 23] of those schemes the numerical f ux of the Q-scheme can be recognized. Since the Q-schemes of Bermùdez and Vázquez are particularly designed for conservation laws with source terms of the type considered here, the Roe formulation with entropy f x (RF) and locally Lax–Friedrichs formulation (LLF) are appropriate formulations for the f ux in the presence of source terms.

In the Section 2 we give a brief overview of the well-known ENO-RF, ENO-LLF, WENO-RF, and WENO-LLF schemes for the homogeneous conservation laws in order to introduce

the formulations and notations that we need in the presentation of our modif cations. Then in the Section 3 we expose the new schemes in a general formulation. We apply the schemes to the shallow water equations in Section 4 and discuss other possible applications of the approach. In Section 5 we prove that new schemes have the exact C-property when applied to the shallow water equations. In Section 6 we present results of numerical experiments in several test examples for one-dimensional shallow water equations, which include problems with steady quiescent f ow, steady subcritical f ow, steady transcritical f ow with and without hydraulic jump, near-steady f ow, and rapidly varying f ow. In Section 7 we give some concluding remarks.

2. ENO AND WENO SCHEMES

In this section we give a short overview of the f nite difference ENO and WENO schemes for both the locally Lax–Friedrichs formulation and the Roe with entropy f x formulation. The scope of this overview is to introduce the formulations we need in the presentation of our extension to the source term evaluation. All details about the subject can be found in the numerous references about these classical schemes [1, 7, 8, 12, 13, 19, 21–23].

We consider nonhomogenous hyperbolic systems of conservation laws in one dimension:

$$\partial_t u + \partial_x f(u) = g(u, x). \tag{1}$$

Here t is the time, x is the space coordinate, u is the vector of the conserved variables, f is the f ux, and g is the source term. In fact, the dependence of the source term on the time variable is possible, i.e., the source term can be of the form $g = g(u, x, t)$, but the approach that we develop is aimed at solving diff culties with geometrical source terms.

We rewrite system (1) in the form

$$\partial_t u = L(u, x, t), \tag{2}$$

with L def ned as

$$L(u, x, t) = -\partial_x f(u) + g(u, x). \tag{3}$$

In the ENO and WENO schemes for the time integration in (2) a TVD Runge–Kutta-type method is applied [23].

Furthermore, if an approximation u_i, $i = 0, \ldots, N$, to the solution u at any time t is known, the numerical approximation L_i, $i = 0, \ldots, N$, is found as

$$L_i = -\frac{1}{\Delta x} \left(f_{i+1/2} - f_{i-1/2} \right) + g_i. \tag{4}$$

Here a space discretization with cells $[x_{i-1/2}, x_{i+1/2}]$, $i = 0, \ldots, N$, of uniform width Δx is assumed and the notation $f_{i+1/2}, i = 0, \ldots, N - 1$, for the numerical f ux at the $(i + 1/2)$th cell boundary and g_i, $i = 0, \ldots, N$, for the numerical source term in the ith cell is used. We must point out that f nite difference WENO schemes of third-order accuracy or higher can only be applied to uniform meshes or smoothly varying meshes [20].

In f nite difference ENO and WENO schemes the numerical f ux $f_{i+1/2}$, $i = 0, \ldots,$ $N - 1$, is computed in the following way. First the local characteristic f elds are found, i.e.,

eigenvalues $\lambda_{i+1/2}^{(p)}$, left eigenvectors $l_{i+1/2}^{(p)}$, and right eigenvectors $r_{i+1/2}^{(p)}$, $p = 1, \ldots, m$, are evaluated for the matrix

$$A_{i+1/2} = A(\bar{u}_{i+1/2}), \tag{5}$$

which approximates the local Jacobian matrix of the f ux. Here m is the number of conservation laws in system (1) and $\bar{u}_{i+1/2}$ is some average value of states u_i and u_{i+1}.

Then an ENO or WENO reconstruction algorithm is applied to each characteristic f eld component of the numerical f ux $f_{i+1/2}$. Generally, ENO and WENO reconstruction solves the problem of numerical approximation of a function $v^\pm$ at position $x_{i+1/2}$, if all the values $v_k^\pm$, $k = 0, \ldots, N$, in the cell centers x_k, $k = 0, \ldots, N$, are known. Now we present only three essential facts about ENO and WENO reconstruction (Eqs. (6), (8), and (9)), because we use them in the paper. The complete presentation of these algorithms can be found in [1, 7, 8, 12, 13, 19, 21–23].

First, the f nal result of both the $(r + 1)$th-order ENO and the $(2r + 1)$th-order WENO reconstruction on a uniform mesh of cells can be written as

$$v_{i+1/2,r}^\pm = \sum_{s=s_{\min}^\pm}^{s_{\max}^\pm} \omega_{r,s}(v^\pm) \sum_{j=0}^{r} a_{r,s,j}^\pm v_{i-r+s+j}^\pm. \tag{6}$$

Here the range of indices is bounded with $s_{\min}^+ = 0$, $s_{\max}^+ = r$ or with $s_{\min}^- = 1$, $s_{\max}^- = r + 1$ and $v_k^\pm$ as stated above is the value of the function $v^\pm$ at x_k, $k = 0, \ldots, N$. The coeff cients $a_{r,s,j}^\pm$, $j = 0, \ldots, r$, $s = s_{\min}^\pm, \ldots, s_{\max}^\pm$, have known values that for example can be found in [23]. Each weight $\omega_{r,s}(v^\pm)$, $s = s_{\min}^\pm, \ldots, s_{\max}^\pm$, is computed from some smoothness indicator that measures smoothness of the function $v^\pm$ over the sth stencil of points

$$S_{r,s}^\pm = \{x_{i-r+s}, \ldots, x_{i+s}\}, \quad s = s_{\min}^\pm, \ldots, s_{\max}^\pm. \tag{7}$$

The only difference between the ENO and WENO algorithm is in the evaluation of the weights. In the ENO reconstruction only one stencil is chosen for the reconstruction; i.e., for this stencil the weight is equal to 1 and all the other stencils have zero weight. In the WENO reconstruction the weight values are distributed more evenly and are normalized, i.e., the sum of weights is equal to 1. Even more, we can easily see that in both cases

$$\sum_{s=s_{\min}^\pm}^{s_{\max}^\pm} \omega_{r,s}(v^\pm) \sum_{j=0}^{r} a_{r,s,j}^\pm = 1. \tag{8}$$

This is the second fact that we want to emphasize. The last fact regarding ENO and WENO reconstructions that we need is that values of the weights do not change if any constant value is added to the function; i.e.,

$$\omega_{r,s}(v^\pm + const.) = \omega_{r,s}(v^\pm), \quad s = s_{\min}^\pm, \ldots, s_{\max}^\pm. \tag{9}$$

In the ENO reconstruction the choice of stencil is based on divided differences from f rst order up, and in the WENO reconstruction smoothness indicators use only derivatives of the interpolation polynomial from f rst order up. This can all be easily verif ed in

Refs. [1, 7, 8, 12, 13, 19, 21–23] and it is a logical property of the weights since smoothness of a function does not change with translation.

Now, we can explain how the ENO or WENO reconstruction algorithms can be applied to the evaluation of the numerical f ux. Actually we present the LLF and the RF versions of the ENO and WENO scheme in a form that is not common; i.e., in the next two subsections we present the transition from the classical to the formulation we need. The advantages of the reformulations become clear in Sections 3 and 4.

2.1. *LLF Flux Formulations*

In the ENO-LLF and WENO-LLF schemes, in order to numerically approximate the f ux component for each $(i + 1/2)$th cell boundary and each pth characteristic f eld two functions $v^\pm$ are def ned by

$$v^\pm = \frac{1}{2}\left(\boldsymbol{f} \pm \alpha_{i+1/2}^{(p)}\boldsymbol{u}\right) \cdot \boldsymbol{l}_{i+1/2}^{(p)}, \tag{10}$$

where $\alpha_{i+1/2}^{(p)}$ is a numerical approximation for the $\max_{[x_i, x_{i+1}]}|\lambda^{(p)}|$; for example

$$\alpha_{i+1/2}^{(p)} = \max\left(|\lambda_i^{(p)}|, |\lambda_{i+1}^{(p)}|, |\lambda_{i+1/2}^{(p)}|\right). \tag{11}$$

Here $\lambda_i^{(p)} = \lambda^{(p)}(\boldsymbol{u}_i)$. Then values $v_{i+1/2,r}^\pm$ are computed using the $(r + 1)$th-order ENO or the $(2r + 1)$th-order WENO reconstruction, i.e., as given with (6), and the f ux component is set to

$$f_{i+1/2}^{(p)} = v_{i+1/2,r}^+ + v_{i+1/2,r}^-. \tag{12}$$

We want to note that obviously the functions $v^\pm$ depend on the cell boundary and on the local characteristic f eld. However, we do not add subscripts $i + 1/2$ and p to its names in (10) in order to diminish the total number of subscripts and to make clearer the application of ENO or WENO reconstruction algorithm. We use similar abbreviations in the next sections too.

Now we want to reformulate these expressions in order to prepare the balancing we present in Section 3. In fact we can relate the building blocks (10) of the LLF formulation with the numerical f ux component of the Q-schemes

$$f_{i+1/2}^{(p)} = \frac{1}{2}\left((\boldsymbol{f}_i + \boldsymbol{f}_{i+1}) - |\lambda_{i+1/2}^{(p)}|(\boldsymbol{u}_{i+1} - \boldsymbol{u}_i)\right) \cdot \boldsymbol{l}_{i+1/2}^{(p)} \tag{13}$$

if instead of (11) we take

$$\alpha_{i+1/2}^{(p)} = |\lambda_{i+1/2}^{(p)}|. \tag{14}$$

Using this we can rewrite (12) as

$$\begin{aligned}
f_{i+1/2}^{(p)} = {} & \frac{1}{2}\left((\boldsymbol{f}_i + \boldsymbol{f}_{i+1}) - \alpha_{i+1/2}^{(p)}(\boldsymbol{u}_{i+1} - \boldsymbol{u}_i)\right) \cdot \boldsymbol{l}_{i+1/2}^{(p)} \\
& + \left(v_{i+1/2,r}^+ - \frac{1}{2}\left(\boldsymbol{f}_i + \alpha_{i+1/2}^{(p)}\boldsymbol{u}_i\right) \cdot \boldsymbol{l}_{i+1/2}^{(p)}\right) \\
& + \left(v_{i+1/2,r}^- - \frac{1}{2}\left(\boldsymbol{f}_{i+1} - \alpha_{i+1/2}^{(p)}\boldsymbol{u}_{i+1}\right) \cdot \boldsymbol{l}_{i+1/2}^{(p)}\right).
\end{aligned} \tag{15}$$

Then we can introduce two terms $P_{i+1/2,\pm}^{(p)}$ for the two expressions in brackets in the second and third line of (15). From (15) we can see that these terms are actually high-order ENO or WENO corrections of the f rst-order Q-scheme. If we now use (6) and (8) we f nd that

$$P_{i+1/2,\pm}^{(p)} = \sum_{s=s_{min}^{\pm}}^{s_{max}^{\pm}} \sum_{j=0}^{r} \omega_{r,s}(v^{\pm}) a_{r,s,j}^{\pm} \hat{v}_{i-r+s+j}^{\pm}, \tag{16}$$

with new functions $\hat{v}^{\pm}$ def ned as

$$\hat{v}^{\pm} = \frac{1}{2}\left(\left(\boldsymbol{f} \pm \alpha_{i+1/2}^{(p)} \boldsymbol{u}\right) - \left(\boldsymbol{f}_{I^{\pm}} \pm \alpha_{i+1/2}^{(p)} \boldsymbol{u}_{I^{\pm}}\right)\right) \cdot \boldsymbol{l}_{i+1/2}^{(p)}. \tag{17}$$

Here we introduce

$$I^{+} = i, \quad I^{-} = i + 1. \tag{18}$$

We can see that functions $v^{\pm}$ and $\hat{v}^{\pm}$ differ only by a constant value. Now (9) leads to

$$\omega_{r,s}(v^{\pm}) = \omega_{r,s}(\hat{v}^{\pm}), \quad s = s_{min}^{\pm}, \dots, s_{max}^{\pm}, \tag{19}$$

so $P_{i+1/2,\pm}^{(p)}$ are exactly ENO or WENO reconstructions for functions $\hat{v}^{\pm}$.

With this we obtain the equivalent form of the LLF algorithm that can be f nally written as follows. The ENO-LLF and WENO-LLF numerical approximation for the f ux component for each $(i + 1/2)$th cell boundary and each pth characteristic f eld is

$$f_{i+1/2}^{(p)} = \frac{1}{2}\left((\boldsymbol{f}_i + \boldsymbol{f}_{i+1}) - \alpha_{i+1/2}^{(p)}(\boldsymbol{u}_{i+1} - \boldsymbol{u}_i)\right) \cdot \boldsymbol{l}_{i+1/2}^{(p)} + P_{i+1/2,+}^{(p)} + P_{i+1/2,-}^{(p)}, \tag{20}$$

$$P_{i+1/2,\pm}^{(p)} = \sum_{s=s_{min}^{\pm}}^{s_{max}^{\pm}} \sum_{j=0}^{r} \omega_{r,s}(\hat{v}^{\pm}) a_{r,s,j}^{\pm} \hat{v}_{i-r+s+j}^{\pm}, \tag{21}$$

with functions $\hat{v}^{\pm}$ as def ned in (17).

2.2. *RF Flux Formulations*

In the RF algorithm the entropy f x is applied for the f ux component at the $(i + 1/2)$th cell boundary and in the pth characteristic f eld if the eigenvalue changes sign, i.e., if $\lambda_i^{(p)}\lambda_{i+1}^{(p)} \leq 0$. In this case the entropy f x consists of applying the LLF formulation that we already stated and reformulated. So in this subsection we concentrate only on the pure Roe formulation. We emphasize that in the RF formulation it is applied only if $\lambda_i^{(p)}\lambda_{i+1}^{(p)} > 0$.

In the Roe formulation the numerical approximation of the f ux component for each $(i + 1/2)$th cell boundary and each pth characteristic f eld is equal to the sum of the ENO or WENO reconstruction at $x_{i+1/2}$ of two functions

$$v^{\pm} = \frac{1 \pm \mathrm{sgn}\left(\lambda_{i+1/2}^{(p)}\right)}{2} \boldsymbol{f} \cdot \boldsymbol{l}_{i+1/2}^{(p)}. \tag{22}$$

We again reformulate this algorithm in order to prepare it for the balancing. Particularly we can associate the building block (22) with the simple upwind scheme

$$f_{i+1/2}^{(p)} = \begin{cases} \boldsymbol{f}_i \cdot \boldsymbol{l}_{i+1/2}^{(p)} & \text{if } \lambda_{i+1/2}^{(p)} > 0 \\ \boldsymbol{f}_{i+1} \cdot \boldsymbol{l}_{i+1/2}^{(p)} & \text{otherwise.} \end{cases} \tag{23}$$

Now with a sequence of arguments similar to that for the LLF case, which we here omit, we can f nd the needed reformulation. The f nal result is that the ENO-Roe or WENO-Roe numerical approximation for the f ux component for each $(i + 1/2)$th cell boundary and each pth characteristic f eld is given by

$$f_{i+1/2}^{(p)} = \begin{cases} \boldsymbol{f}_i \cdot \boldsymbol{l}_{i+1/2}^{(p)} + P_{i+1/2,+}^{(p)} & \text{if } \lambda_{i+1/2}^{(p)} > 0 \\ \boldsymbol{f}_{i+1} \cdot \boldsymbol{l}_{i+1/2}^{(p)} + P_{i+1/2,-}^{(p)} & \text{otherwise,} \end{cases} \tag{24}$$

with $P_{i+1/2,\pm}^{(p)}$ def ned with (21), but not for functions $\hat{v}^\pm$ def ned with

$$\hat{v}^\pm = \frac{1 \pm \text{sgn}(\lambda_{i+1/2}^{(p)})}{2}(\boldsymbol{f} - \boldsymbol{f}_{I^\pm}) \cdot \boldsymbol{l}_{i+1/2}^{(p)}, \tag{25}$$

instead of (17).

3. BALANCING OF THE FLUX GRADIENT AND THE SOURCE TERM

In this section we propose a modif cation of the ENO and WENO schemes. This modif cation has no effect if the hyperbolic conservation law system is homogeneous, but when the source term is present it affects the numerical approximation of the f ux and not just of the source term. It is based on the idea of balancing the f ux gradient and the source term [3], and its f nal formulation depends on the conservation law system to which it is applied.

From now on the ENO and WENO schemes with the f ux evaluated as described in Section 2 and the source term evaluated pointwise we call the ENO and WENO schemes with source term added, while we refer to the modif ed schemes as the ENO and WENO schemes with source term decomposed.

3.1. LLF Formulation with Source Term Decomposed

In Q-schemes of Bermùdez and Vázquez the balancing between the f ux gradient and source term is obtained by using (13) for the numerical f ux, by decomposing the source term

$$g_i^{(p)} = g_{i+1/2,L}^{(p)} + g_{i-1/2,R}^{(p)}, \tag{26}$$

and by applying upwinding to the decomposed parts

$$g_{i+1/2,L}^{(p)} = \frac{1 - \text{sgn}(\lambda_{i+1/2}^{(p)})}{2\Delta x} \boldsymbol{G}(\boldsymbol{u}_i, \boldsymbol{u}_{i+1}, x_i, x_{i+1}) \cdot \boldsymbol{l}_{i+1/2}^{(p)}, \tag{27}$$

$$g_{i+1/2,R}^{(p)} = \frac{1 + \text{sgn}(\lambda_{i+1/2}^{(p)})}{2\Delta x} \boldsymbol{G}(\boldsymbol{u}_i, \boldsymbol{u}_{i+1}, x_i, x_{i+1}) \cdot \boldsymbol{l}_{i+1/2}^{(p)}. \tag{28}$$

Here the function $G(u', u'', x', x'')$ is constructed from the source term of the conservation law and its formulation is crucial for the balancing [2, 3]. We give the shallow water case as well as some general idea about its construction in the Section 4.

If we look at our reformulation (20) of the LLF algorithm we can see that it contains the Q-scheme part that can obviously be balanced with (26)–(28), but also the ENO or WENO reconstruction terms $P_{i+1/2,\pm}^{(p)}$ that need additional balancing. In order to achieve this we introduce new terms $Q_{i+1/2,\pm}^{(p)}$ and propose substituting (27) and (28) with

$$g_{i+1/2,L}^{(p)} = \frac{1 - \text{sgn}(\lambda_{i+1/2}^{(p)})}{2\Delta x} G(u_i, u_{i+1}, x_i, x_{i+1}) \cdot l_{i+1/2}^{(p)} + \frac{1}{\Delta x} Q_{i+1/2,+}^{(p)} + \frac{1}{\Delta x} Q_{i+1/2,-}^{(p)},$$

(29)

$$g_{i+1/2,R}^{(p)} = \frac{1 + \text{sgn}(\lambda_{i+1/2}^{(p)})}{2\Delta x} G(u_i, u_{i+1}, x_i, x_{i+1}) \cdot l_{i+1/2}^{(p)} - \frac{1}{\Delta x} Q_{i+1/2,+}^{(p)} - \frac{1}{\Delta x} Q_{i+1/2,-}^{(p)}.$$

(30)

We must emphasize that def nitions (29) and (30) (and later (34) and (35)) bound the developed algorithm exclusively to uniform meshes.

Only examination of the def nition (21) of the terms $P_{i+1/2,\pm}^{(p)}$ can lead us to the necessary def nition of the terms $Q_{i+1/2,\pm}^{(p)}$. We propose using an expression similar to (21); we propose even more using the same weights for $P_{i+1/2,\pm}^{(p)}$ and for $Q_{i+1/2,\pm}^{(p)}$ and in this way reducing the problem of balancing to the balancing between the functions $\hat{v}^\pm$ for f ux with some appropriately def ned functions $\hat{w}^\pm$ for the source term. Def nition (17) now shows the second advantage of our reformulation of the standard LLF algorithm. Since in the conservation law the balance is between the source and the f ux gradient, the numerical method can preserve this property by creating balance between the numerical source and the f nite difference of the numerical f ux. Our functions $\hat{v}^\pm$ already contain differences of f uxes so they can be easily balanced if we def ne the new functions $\hat{w}^\pm$

$$\hat{w}^\pm = \frac{1}{2}\left(G(u_{I^\pm}, u, x_{I^\pm}, x) \pm \text{sgn}(\lambda_{i+1/2}^{(p)})\beta_{i+1/2} Z(u_{I^\pm}, u, x_{I^\pm}, x)\right) \cdot l_{i+1/2}^{(p)}.$$

(31)

Here the expressions for term $\beta_{i+1/2}$ and for the function $Z(u', u'', x', x'')$ are also conservation law dependent and we describe their construction in Section 4.

Now we are left with only one problem to solve: the weights of the stencils. We know that they are derived from the smoothness indicators and their purpose is to diminish inf uence of the stencils over which the f ux is less smooth. But if the reason for the lower smoothness is in the source term and if it is actually balanced with it, then it is wrong to give to such a stencil a smaller weight value. So, we propose evaluating weights from the difference $\hat{v}^\pm - \hat{w}^\pm$. This f nally leads us to the new def nitions for $P_{i+1/2,\pm}^{(p)}$ and $Q_{i+1/2,\pm}^{(p)}$:

$$P_{i+1/2,\pm}^{(p)} = \sum_{s=s_{\min}^\pm}^{s_{\max}^\pm} \sum_{j=0}^{r} \omega_{r,s}(\hat{v}^\pm - \hat{w}^\pm)a_{r,s,j}^\pm \hat{v}_{i-r+s+j}^\pm,$$

(32)

$$Q_{i+1/2,\pm}^{(p)} = \sum_{s=s_{\min}^\pm}^{s_{\max}^\pm} \sum_{j=0}^{r} \omega_{r,s}(\hat{v}^\pm - \hat{w}^\pm)a_{r,s,j}^\pm \hat{w}_{i-r+s+j}^\pm.$$

(33)

It is important to notice that in (4) the difference $P^{(p)}_{i+1/2,\pm} - Q^{(p)}_{i+1/2,\pm}$ appears, which is exactly the ENO or WENO reconstruction for $\hat{v}^\pm - \hat{w}^\pm$.

3.2. *RF Formulation with Source Term Decomposed*

Here again, as in Section 2.2, since the entropy f x means application of LLF formulation if $\lambda^{(p)}_i \lambda^{(p)}_{i+1} \leq 0$ we concentrate only on the pure Roe formulation.

It is easy to verify that the simple upwind scheme (23) can also be balanced with (27) and (28). So, completely analogous thinking, as in the LLF case, leads us to the new Roe algorithm: def ne f ux with (24), (25), and (32), and def ne the source term with (26),

$$g^{(p)}_{i+1/2,L} = \frac{1 - \mathrm{sgn}\left(\lambda^{(p)}_{i+1/2}\right)}{2\Delta x} G(u_i, u_{i+1}, x_i, x_{i+1}) \cdot l^{(p)}_{i+1/2} + \frac{1}{\Delta x} Q^{(p)}_{i+1/2,+}, \tag{34}$$

$$g^{(p)}_{i+1/2,R} = \frac{1 + \mathrm{sgn}\left(\lambda^{(p)}_{i+1/2}\right)}{2\Delta x} G(u_i, u_{i+1}, x_i, x_{i+1}) \cdot l^{(p)}_{i+1/2} - \frac{1}{\Delta x} Q^{(p)}_{i+1/2,-}, \tag{35}$$

and (33) where functions $\hat{w}^\pm$ are now def ned as

$$\hat{w}^\pm = \frac{1 \pm \mathrm{sgn}\left(\lambda^{(p)}_{i+1/2}\right)}{2} G(u_{I^\pm}, u, x_{I^\pm}, x) \cdot l^{(p)}_{i+1/2}. \tag{36}$$

4. APPLICATION TO THE SHALLOW WATER EQUATIONS

In this section we apply the algorithm developed in Section 3 to one-dimensional shallow water equations, give a brief idea of the almost straightforward extension to multidimension, particularly two-dimensional shallow water equations, and emphasize the limitation regarding the application to conservation laws with spatially dependent f uxes.

One case of the hyperbolic conservation laws system (1) with

$$u = \begin{pmatrix} h \\ hv \end{pmatrix}, \quad f = \begin{pmatrix} hv \\ hv^2 + \frac{1}{2}gh^2 \end{pmatrix}, \quad \text{and} \quad g = \begin{pmatrix} 0 \\ gh\left(-\frac{dz}{dx} - \frac{M^2 v|v|}{h^{4/3}}\right) \end{pmatrix} \tag{37}$$

is the one-dimensional St. Venant equations system, i.e., the one-dimensional shallow water equations. Here $h = h(x, t)$ is the water depth, $v = v(x, t)$ is the water velocity, g is the acceleration due to gravity, $z = z(x)$ is the bed level, and $M = M(x)$ is the Manning's friction factor.

According to previous sections now we need to choose the average value $\bar{u}_{i+1/2}$ in (5) and def ne terms $G(u', u'', x', x'')$, $Z(u', u'', x', x'')$, and $\beta_{i+1/2}$. We take

$$\bar{u}_{i+1/2} = \frac{u_i + u_{i+1}}{2}. \tag{38}$$

The verif cation of the exact C-property depends on this particular choice, as it will be shown.

Furthermore, since the part of the source term concerning friction forces does not produce numerical diff culties when evaluated pointwise, we apply decomposition only to the part

of the source term due to gravitational forces ($\begin{smallmatrix} 0 \\ -gh\frac{dz}{dx} \end{smallmatrix}$) and we evaluate the friction term ($\begin{smallmatrix} 0 \\ -gh\frac{M^2 v|v|}{h^{4/3}} \end{smallmatrix}$) pointwise.

The formulations for $G(u', u'', x', x'')$, $Z(u', u'', x', x'')$, and $\beta_{i+1/2}$ that we introduce are

$$G(u', u'', x', x'') = \begin{pmatrix} 0 \\ -g\frac{h'+h''}{2}(z(x'') - z(x')) \end{pmatrix}, \tag{39}$$

$$Z(u', u'', x', x'') = \begin{pmatrix} 0 \\ -(z(x'') - z(x')) \end{pmatrix}, \tag{40}$$

$$\beta_{i+1/2} = g\overline{h}_{i+1/2}. \tag{41}$$

A general idea about this construction is as follows. In order to get $G(u', u'', x', x'')$ the gradient of some geometrical property that appears in the source term should be substituted with its f nite difference, and the state variables with the same average values that are used for the computation of the local characteristic f eld. Furthermore, term $\beta_{i+1/2}$ must create balance with term $\alpha_{i+1/2}^{(p)}$, and function $Z(u', u'', x', x'')$ should contain only the f nite difference of the geometrical property.

Now, we can discuss possible other applications of the algorithm. One extension of the one-dimensional shallow water equations, (1) and (37), is the one-dimensional shallow water equations in channels with irregular geometry [9, 25]. Particularly for an open channel with variable breadth and a locally rectangular cross section these equations are obtained by placing

$$u = \begin{pmatrix} Bh \\ Bhv \end{pmatrix}, \quad f = \begin{pmatrix} Bhv \\ Bhv^2 + \frac{1}{2}gBh^2 \end{pmatrix}, \quad \text{and}$$

$$g = \begin{pmatrix} 0 \\ \frac{1}{2}gh^2\frac{dB}{dx} + gBh\left(-\frac{dz}{dx} - \frac{M^2 v|v|}{R_h^{4/3}}\right) \end{pmatrix} \tag{42}$$

in (1). Here the notation is the same as in (37) with an additional $B = B(x)$ for the channel breadth and R_h for the hydraulic radius. However, an application of the approach presented in Section 3 is not possible. We must notice that the f ux term in (42) is spatially dependent, i.e., $f = f(u, x)$, since it contains explicit dependency on the space variable through the channel breadth term. The locally Lax–Friedrichs and Roe formulation used for the f ux in ENO and WENO schemes are not appropriate for spatially dependent f uxes. So an extension of the proposed approach would be needed, beginning with a modif cation of the numerical approximation for the f ux, and only then could a balancing between the f ux gradient and the source term be applied. Some preliminary results we have show that this can be done but an adequate algorithm differs so much from the one presented in Sections 2 and 3 that its presentation goes beyond the scope of this paper.

A quite simple extension of the presented algorithm to multidimensions can be done if the hyperbolic conservation law system is of the form

$$\partial_t u + \sum_{k=1}^{d} \partial_{x_k} f_k(u) = \sum_{k=1}^{d} g_k(u, x), \tag{43}$$

i.e., if the source term can be written as a sum of terms of which each balances the f ux gradient in the appropriate direction. Here d is the number of space dimensions, and

$x = (x_1, \ldots, x_d)$ is the space variable. For example two-dimensional shallow water equations without friction are of the form (43) with

$$
\boldsymbol{u} = \begin{pmatrix} h \\ hv_1 \\ hv_2 \end{pmatrix}, \quad \boldsymbol{f}_1 = \begin{pmatrix} hv_1 \\ hv_1^2 + \frac{1}{2}gh^2 \\ hv_1v_2 \end{pmatrix}, \quad \boldsymbol{f}_2 = \begin{pmatrix} hv_2 \\ hv_1v_2 \\ hv_2^2 + \frac{1}{2}gh^2 \end{pmatrix}, \quad (44a)
$$

$$
\boldsymbol{g}_1 = \begin{pmatrix} 0 \\ -gh\frac{\partial z}{\partial x_1} \\ 0 \end{pmatrix}, \quad \text{and} \quad \boldsymbol{g}_2 = \begin{pmatrix} 0 \\ 0 \\ -gh\frac{\partial z}{\partial x_2} \end{pmatrix}. \quad (44b)
$$

Here $h = h(\boldsymbol{x}, t)$ is the water depth, $\boldsymbol{v} = (v_1(\boldsymbol{x}, t), v_2(\boldsymbol{x}, t))$ is the water velocity, g is the acceleration due to gravity, and $z = z(\boldsymbol{x})$ is the bed level. In that case we can apply the algorithm of Section 3 to each direction separately, i.e., to each pair $\boldsymbol{f}_k, \boldsymbol{g}_k$. This is consistent with the usual strategy in ENO and WENO schemes when applied to multidimensional problems ([1, 7, 8, 12, 13, 19, 21–23]). However, this extension has several drawbacks in practical computations since it results in a f nite difference method that can be applied only to uniform meshes and since higher order ENO and WENO schemes with the source term decomposed in multidimension are certainly very computationally expensive.

Another class of conservation laws to which proposed schemes might be applicable includes Euler equations with stiff source terms. Particularly this is true for nozzle f ow equations since in that conservation law system the cross-section area of the nozzle through which ideal gas f ows has a function analogous to the channel width in the open channel f ow equations for a channel with variable width and rectangular cross section (42). There is also the possibility of application to chemically reactive Euler equations [11]. However, further investigation is needed in order to achieve results in those cases and very likely some extensions of the presented algorithms will be necessary.

Since with this we presented the algorithms of the new schemes, we can now discuss the similarities and differences with several other schemes.

Another scheme that is based on the Q-schemes of Bermùdez and Vázquez is the f ux limited scheme with source term decomposed of Hubbard and Garcia-Navarro [9]. The difference consists of the fact that there, high resolution is obtained through a f ux limiting technique instead of through ENO or WENO reconstruction. Therefore the f ux limited schemes are of second-order accuracy, while these schemes achieve higher orders (test problem in Section 6.1).

Comparison with LeVeque's quasi-steady wave propagation algorithm [16, 17] gives the following conclusions. The here-proposed schemes, just like the Q-scheme, decomposes the source term from cell center to cell boundaries and in a way "mimics" the discretization of the f ux term. On the other hand LeVeque introduces an additional Riemann problem at each cell center and obtains balance by implying that its f ux difference must exactly cancel the source term. In particular, if we compare the approximate Riemann solvers in the homogenous case, we can see that the Q-scheme with the Roe average and LeVeque's scheme are equivalent. In the case of linear systems with the source term present these two schemes also coincide. The similarity lies also in the applicability of the compared schemes to the same group of conservation laws, i.e., those with geometrical source terms, particularly to shallowwater equations. The difference is that for those conservation laws the

Q-scheme and our ENO and WENO extensions have the exact C-property, while LeVeque's scheme has the approximate C-property.

Further comparison can be done with Jenny and Müller's Rankine–Hugoniot–Riemann solver [11]. The similarity is in the viewing of the source term as concentrated at cell boundaries, i.e., in applying upwinding to source terms. The difference is in the solver; they use a characteristic-based Rankine–Hugoniot–Riemann solver. Also, since these authors apply their scheme to reacting f ows they do not deal with geometrical dependences in the source term and therefore for their scheme the notion of the exact C-property is not relevant.

Particularly interesting is the comparison with Smolarkiewicz's MPDATA schemes. On one level the difference is in the treatment of the f ux term. Our schemes inherit it from ENO and WENO schemes, which emphasize the nonoscillatory polynomial reconstruction, while MPDATA are advection algorithms that achieve high order through iterative extension of the donor cell schemes. The second level is the numerical modeling of the source term. Obviously this is the main concern of our new algorithm and it consists of the implementation of the f ux gradient source term balancing in ENO and WENO schemes. In the MPDATA schemes there are two important things to be noticed regarding this problem. First is that state-of-the-art MPADATA schemes improve on the time truncation error due to right-hand side numerical modeling, which can be interpreted as integration of the right-hand side along the particle path instead of a central-in-time evaluation. But what is particularly interesting to observe is its application to shallow water models. As we can see in [24], if the model of the shallow f uid on sphere is simplif ed to a shallow water model with noncurvilinear coordinates the MPDATA schemes have the exact C-property. Actually, in order to apply the advection algorithm approach in these schemes the shallow water equations are not written as in (37); i.e., the term $\frac{1}{2}gh^2$ is placed not in the f ux but on the right-hand side, which therefore contains the spatial derivative of the water level instead of the bed alone. This leads straightforwardly to verif cation of the exact C-property of the MPDATA schemes.

Finally, some analogy can be found also in comparison to the surface gradient method developed by Zhou *et al.* [26]. In fact, even if they use pointwise evaluation of the source term Zhou *et al.* obtain a well-balanced scheme since for the computation of the linearly extrapolated states on the cell interfaces they use water level gradient instead of elevation gradient. In our algorithm the choice of stencil weights in (32) and (33) follows funda- mentally the same idea—the weights indirectly measure discontinuities in the water level instead of discontinuities in the elevation.

5. EXACT CONSERVATION PROPERTY FOR SHALLOW WATER EQUATIONS

The def nition of the exact conservation property of a numerical scheme for shallow water equations as given in [2, 3] is the following: *a scheme is said to satisfy the exact C-property if it is exactly compatible with the quiescent steady-state solution*

$$h + z = H = const. \quad \text{and} \quad v = 0. \tag{45}$$

In this section we prove that the ENO and WENO schemes with the source term de- composed, as proposed in Section 3 together with the relations (38)–(41), when applied to the one-dimensional shallow water equations, have this exact C-property. The proof for the

two-dimensional case is completely analogous, so we omit it. We also discuss the order of accuracy of the new schemes.

First we observe that in the case of the quiescent steady-state solution, the f ux and the source term reduce to

$$f = \begin{pmatrix} 0 \\ \frac{1}{2}gh^2 \end{pmatrix}, \quad g = \begin{pmatrix} 0 \\ -gh\frac{dz}{dx} \end{pmatrix}, \tag{46}$$

while eigenvalues and right and left eigenvectors reduce to

$$\lambda^{(p)} = (-1)^p c, \quad r^{(p)} = \begin{pmatrix} 1 \\ (-1)^p c \end{pmatrix}, \quad l^{(p)} = \frac{1}{2c}\begin{pmatrix} c \\ (-1)^p \end{pmatrix}, \quad p=1,2, \tag{47}$$

where $c = \sqrt{gh}$. The proof of the exact C-property consists of demonstrating that if condition (45) is valid, then $L_i = 0, i = 0, \ldots, N$. According to our construction of the new schemes in Section 3, it is obvious that verif cation of the exact C-property depends only on verifying whether

$$\hat{v}_k^{\pm} - \hat{w}_k^{\pm} = 0, \quad k = 0, \ldots, N \tag{48}$$

is true under quiescent f ow conditions (45). Now we study the two schemes separately.

5.1. *Exact C-Property of the LLF Formulation with Source Term Decomposed*

For the LLF formulation, f rst we can compute the part

$$(f_k - f_{I^{\pm}}) - G(u_{I^{\pm}}, u_k, x_{I^{\pm}}, x_k) = \begin{pmatrix} 0 \\ \frac{1}{2}gh_k^2 - \frac{1}{2}gh_{I^{\pm}}^2 \end{pmatrix} - \begin{pmatrix} 0 \\ -g\frac{h_{I^{\pm}}+h_k}{2}(z_k - z_{I^{\pm}}) \end{pmatrix} \tag{49}$$

of $\hat{v}_k^{\pm} - \hat{w}_k^{\pm}$, and this becomes

$$(f_k - f_{I^{\pm}}) - G(u_{I^{\pm}}, u_k, x_{I^{\pm}}, x_k) = \begin{pmatrix} 0 \\ g\frac{h_{I^{\pm}}+h_k}{2}(H_k - H_{I^{\pm}}) \end{pmatrix} = 0 \tag{50}$$

in the quiescent f ow case.

Second, let us observe that for the quiescent f ow

$$\alpha_{i+1/2}^{(p)} = |\lambda_{i+1/2}^{(p)}| = \bar{c}_{i+1/2}, \tag{51}$$

$$\text{sgn}(\lambda_{i+1/2}^{(p)})\beta_{i+1/2} = (-1)^p \bar{c}_{i+1/2}^2; \tag{52}$$

so, simple computation for the second part of $\hat{v}_k^{\pm} - \hat{w}_k^{\pm}$,

$$\left(\alpha_{i+1/2}^{(p)}(u_k - u_{I^{\pm}}) - \text{sgn}(\lambda_{i+1/2}^{(p)})\beta_{i+1/2}Z(u_{I^{\pm}}, u_k, x_{I^{\pm}}, x_k)\right) \cdot l_{i+1/2}^{(p)}$$

$$= \frac{1}{2\bar{c}_{i+1/2}}\left(\begin{pmatrix} \bar{c}_{i+1/2}(h_k - h_{I^{\pm}}) \\ 0 \end{pmatrix} - \begin{pmatrix} 0 \\ -(-1)^p \bar{c}_{i+1/2}^2(z_k - z_{I^{\pm}}) \end{pmatrix}\right) \cdot \begin{pmatrix} \bar{c}_{i+1/2} \\ (-1)^p \end{pmatrix}, \tag{53}$$

gives us that under (45)

$$\left(\alpha_{i+1/2}^{(p)}(\boldsymbol{u}_k - \boldsymbol{u}_{I^\pm}) - \text{sgn}\left(\lambda_{i+1/2}^{(p)}\right)\beta_{i+1/2}\boldsymbol{Z}(\boldsymbol{u}_{I^\pm}, \boldsymbol{u}_k, x_{I^\pm}, x_k)\right)\cdot\boldsymbol{l}_{i+1/2}^{(p)}$$

$$= \frac{\overline{c}_{i+1/2}}{2}(H_k - H_{I^\pm}) = 0. \tag{54}$$

So, (48) is a direct consequence of (50) and (54). This proves the exact C-property for the new ENO-LLF and WENO-LLF schemes.

At this point the question of how well the approach works for f ows away from the quiescent steady states arises. Of course we cannot expect a numerical scheme to be exact in the general case, particularly not for the nonsteady case. However, in the case of the nonquiescent steady state the right-hand side in (2) should also be zero, just as in the quiescent case. In particular, analytical integration of the one-dimensional shallow water equations leads us to the relations

$$q = const. \quad \text{and} \quad \frac{1}{2}\frac{q^2}{h^2} + g(h + z) = const., \tag{55}$$

where $q = hv$ is the unit discharge. Computations completely analogous to those for the quiescent state, but with the application of (55) instead of (45), give us

$$((\boldsymbol{f}_k - \boldsymbol{f}_{I^\pm}) - \boldsymbol{G}(\boldsymbol{u}_{I^\pm}, \boldsymbol{u}_k, x_{I^\pm}, x_k))\cdot\boldsymbol{l}_{i+1/2}^{(p)} = \frac{(-1)^{p+1}}{2\overline{c}_{i+1/2}}\frac{q^2}{2h_k^2 h_{I^\pm}^2}(h_k - h_{I^\pm})^3 \tag{56}$$

and

$$\left(\alpha_{i+1/2}^{(p)}(\boldsymbol{u}_k - \boldsymbol{u}_{I^\pm}) - \text{sgn}\left(\lambda_{i+1/2}^{(p)}\right)\beta_{i+1/2}\boldsymbol{Z}(\boldsymbol{u}_{I^\pm}, \boldsymbol{u}_k, x_{I^\pm}, x_k)\right)\cdot\boldsymbol{l}_{i+1/2}^{(p)}$$

$$= \frac{(-1)^{p+1}}{\overline{c}_{i+1/2}}\text{sgn}\left(\lambda_{i+1/2}^{(p)}\right)\left(\frac{q^2}{h_{i+1/2}^2} + \frac{q^2\overline{h}_{i+1/2}}{h_k^2 h_{I^\pm}^2}\frac{h_k + h_{I^\pm}}{2}\right)(h_k - h_{I^\pm}). \tag{57}$$

Equations (56) and (57) show that the proposed ENO-LLF and WENO-LLF schemes with source term decomposed do not exactly conserve the nonquiescent steady states. The same is also true for the Q-schemes.

However we must point out that only few numerical schemes verify the exact C-property and that numerical experiments (Section 6) show very good results on the f ows away from the quiescent case, too. The inclusion of the friction term would additionally complicate the analysis and possible improvements in the schemes regarding the balance for any steady state and with nonzero friction require further study.

5.2. *Exact C-Property of the RF Formulation with Source Term Decomposed*

The same arguments as in the case of the LLF formulations with source term decomposed and the already computed relation (50), valid under quiescent f ow conditions (45), lead to (48). So again the exact C-property is verif ed.

We want to point out here that the proofs of the exact C-property for both cases depend on the choice of the average state evaluation (38). In fact if the Roe average was used only approximate C-property of order 2 could be verif ed [2, 3].

Again, we can compute what happens in the nonquiescent steady-state case. In this algorithm only term (56) appears so ENO-RF and WENO-RF schemes with source term

decomposed also exactly conserve only the quiescent flow and only approximately the nonquiescent steady states.

5.3. Order of Accuracy

In this section we make a few observations regarding the order of accuracy of the new schemes. In particular, let us assume that the solution and the bed slope are smooth enough functions. Then, Rth-order accuracy of the ENO or WENO reconstruction and relations (32) and (33) lead to

$$P_{i+1/2,\pm}^{(p)} = \hat{v}^{\pm}(x_{i+1/2}) + O(\Delta x^R), \tag{58}$$

$$Q_{i+1/2,\pm}^{(p)} = \hat{w}^{\pm}(x_{i+1/2}) + O(\Delta x^R), \tag{59}$$

with $R = r + 1$ in the ENO and $R = 2r + 1$ in the WENO case. In the case of the new LLF algorithms (Section 3.1), Eq. (58) after some simple computation leads to

$$f_{i+1/2}^{(p)} = \boldsymbol{f}_{i+1/2}^* \cdot \boldsymbol{l}_{i+1/2}^{(p)} + O(\Delta x^R). \tag{60}$$

Here $\boldsymbol{f}_{i+1/2}^*$ denotes the exact value of the flux at $x_{i+1/2}$. Similarly, in the case of the new RF algorithms (Section 3.2), (60) is also valid. Thus, the modifications in the algorithm that we introduced do not change the order of the ENO or WENO reconstruction algorithm with respect to the flux term.

When the source term is evaluated pointwise it means that it is exactly evaluated at the cell center so the order of accuracy in the space discretization of WENO schemes is preserved. But in the case of the one-dimensional shallow water equations the source term contains the part due to gravity and the term $\frac{dz}{dx}$ appears. Typically $z = z(x)$ is the known function and in the artificial test problems it can be given as an analytical function so its derivative can be exactly evaluated. But when it is the bed of a natural watercourse $z = z(x)$ is known through a discrete set of data obtained by measurements. So the problem of evaluating $\frac{dz}{dx}$ numerically must be faced and then pointwise evaluation can only mean a first- or second-order-accurate numerical derivative. Since any numerical derivative $z = z(x)$ involves some stencil of points, if the stencil is different from the one used to evaluate the flux in the WENO algorithm or if it is not used with appropriate coefficients the balance between the flux gradient and the source term that is present in the observed physical phenomenon and included in the governing conservation law equations is lost. Only some algorithm that respects this balancing can improve the numerical accuracy and remove numerical errors otherwise present. And this is exactly what is achieved in our algorithm for the ENO and WENO schemes.

6. NUMERICAL RESULTS

In this section we present numerical results for several test problems for the one-dimensional shallow water equations (37). In the computation we apply ENO and WENO schemes with source term decomposed and source term added as we propose them here, as well as Q-schemes of Bermùdez and Vázquez [3] and the flux limited schemes with source term decomposed [9]. In all the computations we chose the time and the space

step according to CFL conditions as well as with the stability conditions given in [3], since the presence of the source term affects the stability of the scheme.

6.1. *A Convergency Test*

The purpose of the first test problem is to numerically test the order of accuracy of the proposed schemes. Since the ENO and WENO schemes when applied to homogenous hyperbolic conservation laws with smooth solutions have high order of accuracy, it is important to see if and how this is modified in the presence of the source term due to the proposed extension of the schemes.

In this convergency test problem the smooth bed is given by

$$z(x) = 0.2 \cdot e^{-\left(\frac{2}{3}(x-10)\right)^2}, \quad x \in [0, 20], \tag{61}$$

the friction is zero, and the initial condition is the steady subcritical flow with the unit discharge $hv(x, 0) = 4.42 \, \text{m}^2/\text{s}$ (Fig. 1). This steady state should be preserved. We know the exact solution since it can be computed using (55). We present results for $t = 50$ s computed with the new ENO-LLF and WENO-LLF schemes, with $r = 1$–5. Similar results are valid also for the RF formulations. In all the computations we apply the CFL coefficient $c_{cfl} = 0.7$. While for $r = 1$ and 2 we apply a two-step Runge–Kutta time integration, for $r = 3$–5 we use a three-step Runge–Kutta time integration. The experimentally established errors and orders for this steady-state flow with smooth bed and solution are given in Table I. Regarding both ENO-LLF and WENO-LLF decomposed schemes we can conclude that they do not achieve the expected formal order but however show a significantly higher order of accuracy in comparison to first- and second-order schemes. The cause of the observed problems and possible remedies require further study.
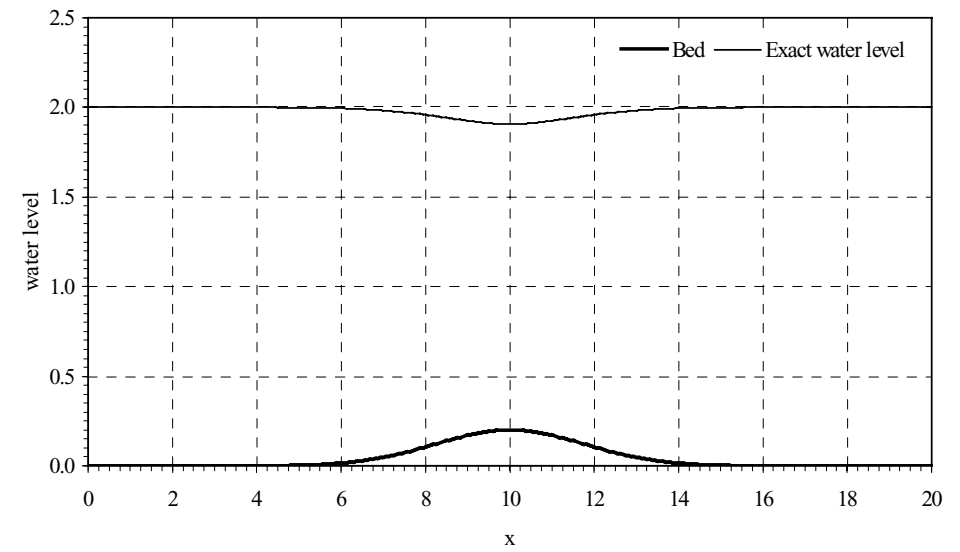

FIG. 1. The exact water level and bed for the steady subcritical flow over a smooth bump (test problem in Section 6.1).

<div align="center">

TABLE I

The Convergency Test Results (Test Problem in Section 6.1)

</div>

		ENO-LLF decomposed		WENO-LLF decomposed	
r	Number of cells	L^1 error	L^1 order	L^1 error	L^1 order
1	20	5.1518×10^{-4}		6.1241×10^{-4}	
	40	1.2691×10^{-4}	2.02	2.9003×10^{-4}	1.08
	80	3.1526×10^{-5}	2.01	4.4874×10^{-5}	2.69
	160	7.8921×10^{-6}	2.00	1.3304×10^{-5}	1.75
	320	1.9332×10^{-6}	2.03	2.3394×10^{-6}	2.51
2	20	7.1908×10^{-3}		7.9906×10^{-3}	
	40	1.5424×10^{-3}	2.22	2.6076×10^{-3}	1.62
	80	3.4132×10^{-4}	2.18	1.7996×10^{-4}	3.86
	160	8.5251×10^{-5}	2.00	7.6440×10^{-6}	4.56
	320	1.9682×10^{-5}	2.11	4.3585×10^{-7}	4.13
3	20	1.2647×10^{-2}		1.1246×10^{-2}	
	40	3.9869×10^{-3}	1.67	1.4051×10^{-3}	3.00
	80	6.4950×10^{-4}	2.62	1.5264×10^{-4}	3.20
	160	1.2185×10^{-4}	2.41	6.6217×10^{-6}	4.53
	320	1.6265×10^{-5}	2.91	1.8550×10^{-7}	5.16
4	20	2.0538×10^{-2}		6.7279×10^{-3}	
	40	4.0899×10^{-3}	2.33	5.5028×10^{-4}	3.61
	80	5.8143×10^{-4}	2.81	2.2359×10^{-5}	4.62
	160	8.4721×10^{-5}	2.78	1.5945×10^{-6}	3.81
	320	1.3918×10^{-5}	2.61	7.8490×10^{-8}	4.34
5	20	3.1595×10^{-2}		4.0166×10^{-3}	
	40	1.9081×10^{-3}	4.05	2.2235×10^{-4}	4.18
	80	4.4742×10^{-4}	2.10	2.4784×10^{-5}	3.17
	160	7.5055×10^{-5}	2.58	7.7136×10^{-7}	5.01
	320	1.9801×10^{-6}	5.24	1.1783×10^{-8}	6.03

6.2. *The Quiescent Flow and a Tidal Wave Propagation over the Bed Proposed by the Working Group on Dam Break Modeling*

In this test problem we use the geometry of the bed that was proposed by the working group on dam break modeling, as described in [9, 25]. The bed slope is discontinuous, so this test problem is a good illustration of the signif cance of the source term decomposition for practical applications to natural watercourses. The values of the bed level are given in [25] and can be seen in Fig. 2, while the friction factor is set to $M = 0.1$. We observe two f ows:

(a) the quiescent steady-state (45) with water level $H = 10$ m and
(b) a tidal wave propagation, where a tidal wave is incoming from the upstream end,

$$h(0, t) = 16 + 4\sin\left(\frac{(t - 10800)\pi}{21600}\right), \tag{62}$$

and a wall is positioned at the downstream boundary, as described in [3]. In both cases we apply the space step $\Delta x = 2.5$ m and the CFL coeff cient $c_{cfl} = 0.8$.

FIG. 2. The bed for the quiescent f ow as proposed by the working group on dam break modeling (test problem in Section 6.2).

In case (a) we perform computations using Q-schemes of Bermùdez and Vázquez [3], f ux limited schemes with source term decomposed [9], and ENO-RF and WENO-RF with source term added and with source term decomposed. All the ENO and WENO schemes we test in a low-order variant, i.e., with a two-step Runge–Kutta-type time integration and with $r = 1$, as well as in a high order variant, i.e., with a three-step Runge–Kutta-type time integration and with $r = 5$. In Table II we present L^∞ error in the water level and in the velocity for all the schemes. Values clearly indicate the effect of the source term decomposition since the nondecomposed schemes present an unacceptably high L^∞ error.

In case (b) we also tested all the mentioned schemes but since errors and accuracy are consistent with the results presented in Table II, we give only numerical results after $t = 10,800$ s for the WENO-RF schemes shown in Fig. 3.

TABLE II

The L_∞ Error for the Quiescent Flow as Proposed by the Working Group on Dam Break Modeling (Test Problem (a) in Section 6.2)

| Method	L^∞ error in water level	L^∞ error in velocity
Q-scheme	Less then 10^{-20}	1.480×10^{-14}
Flux limited scheme	Less then 10^{-20}	5.942×10^{-15}
ENO-RF, $r = 1$, added	5.291×10^{-2}	2.867×10^{-1}
ENO-RF, $r = 1$, decomposed	Less then 10^{-20}	1.222×10^{-14}
ENO-RF, $r = 5$, added	1.668×10^{-1}	4.991×10^{-1}
ENO-RF, $r = 5$, decomposed	1.066×10^{-14}	2.090×10^{-14}
WENO-RF, $r = 1$, added	5.407×10^{-2}	2.667×10^{-1}
WENO-RF, $r = 1$, decomposed	1.954×10^{-14}	4.052×10^{-14}
WENO-RF, $r = 5$, added	8.187×10^{-2}	1.622×10^{-1}
WENO-RF, $r = 5$, decomposed	6.040×10^{-14}	1.010×10^{-13}
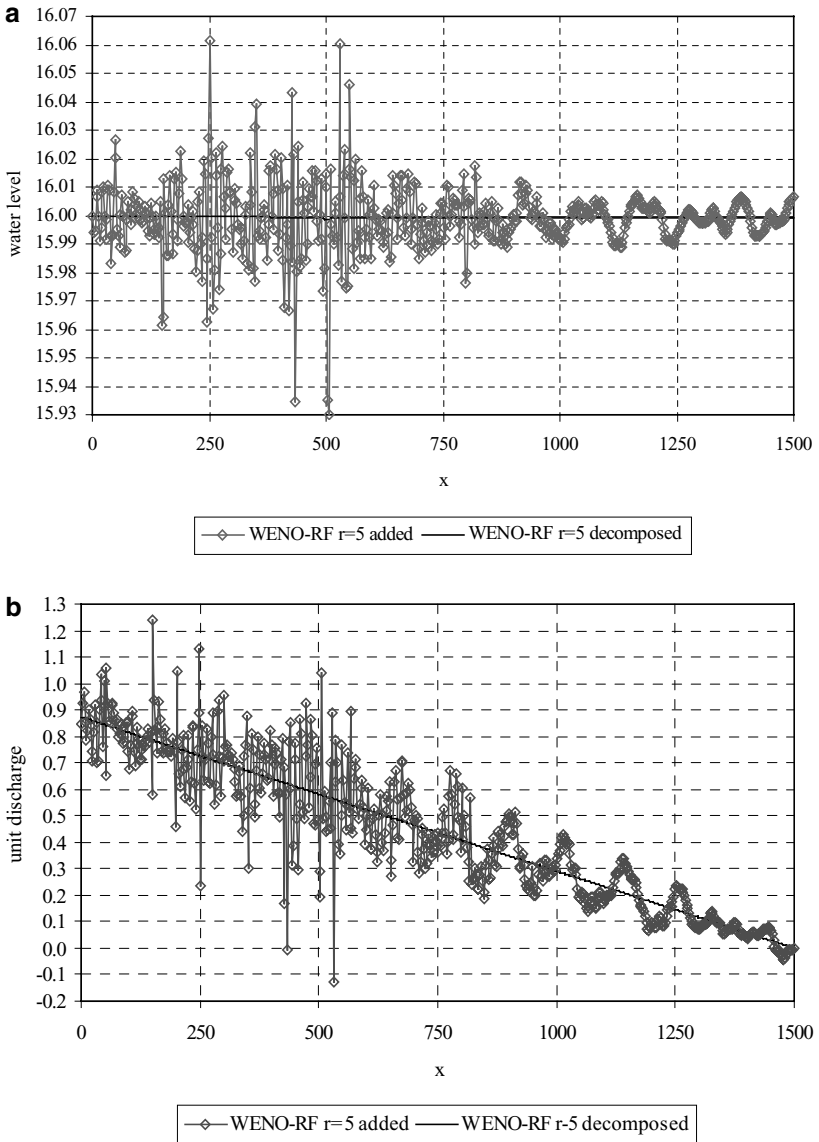
FIG. 3. Comparison of the WENO-RF, $r = 5$, schemes for the tidal wave propagation over the bed proposed by the working group on dam break modeling (test problem (b) in Section 6.2). (a) Water level at $t = 10800$ s; (b) unit discharge at $t = 10800$ s.

6.3. *The Steady Flow over a Bump*

The third test problem covers typical difficulties in the steady shallow water flow, the smooth transition and the hydraulic jump, so it is important for testing the behavior of the new schemes.

The bed in this test problem is given by

$$z(x) = \begin{cases} 0.2 - 0.05(x - 10)^2 & \text{if } 8 \leq x \leq 12 \\ 0 & \text{otherwise,} \end{cases} \tag{63}$$
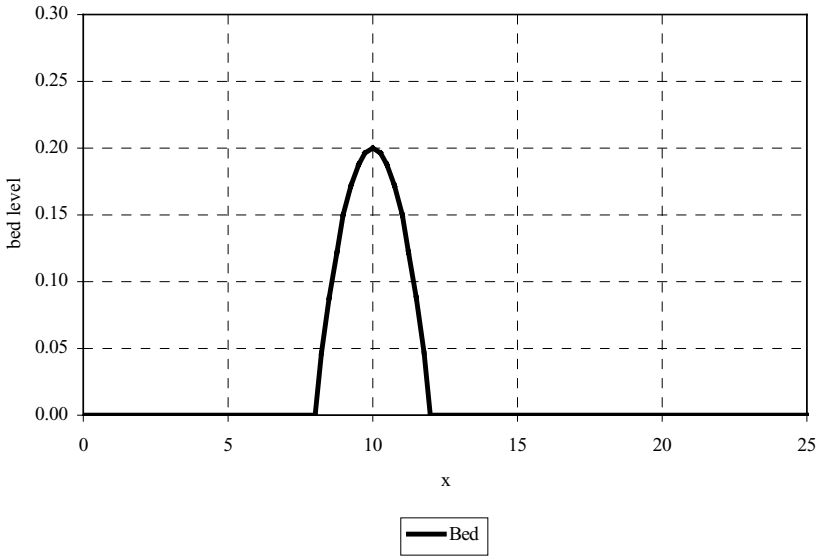
FIG. 4. The bed with a bump (test problem in Section 6.3).

as it can be seen in Fig. 4 [25], and the manning friction factor is set to zero. We impose two different sets of steady boundary conditions:

(a) $hv(0, t) = 0.18 \, \text{m}^2/\text{s}$ and $h(0, t) = 0.33 \, \text{m}$, which results in a steady transcritical f ow with a smooth transition followed by a hydraulic jump, and

(b) $hv(0, t) = 1.53 \, \text{m}^2/\text{s}$, which results in a steady transcritical f ow with a smooth transition.

For both cases we apply the space step $\Delta x = 0.125 \, \text{m}$ and the CFL coeff cient $c_{cfl} = 0.6$. We apply the Q-scheme of Bermùdez and Vázquez [3], the f ux limited schemes with source term decomposed [9], and WENO-RF and WENO-LLF schemes with three-step Runge–Kutta-type time integration and with $r = 5$, with source term added and with source term decomposed. For all these steady f ows exact solutions are known and they are given in [25].

In Fig. 5 we zoom in on the part of the domain where the hydraulic jump occurs in order to make differences between the schemes more visible (Fig. 5a) and we also give a comparison of convergency histories for the applied schemes (Fig. 5b). The global relative error is def ned as in [26], with

$$R = \sqrt{\sum_{i=0}^{N} \left(\frac{h_i^n - h_i^{n-1}}{h_i^n} \right)^2}. \tag{64}$$

The same comparisons can be observed in Fig. 6 for the smooth transition. Furthermore, in Table III we give L^∞ error in the unit discharge for all the applied schemes since these are examples with steady f ow, so the unit discharge should be constant. In particular, in case (a) we give error evaluated on the part of the domain upstream from the jump, since all the tested schemes present the same L^∞ error of magnitude 4×10^{-2} at the jump
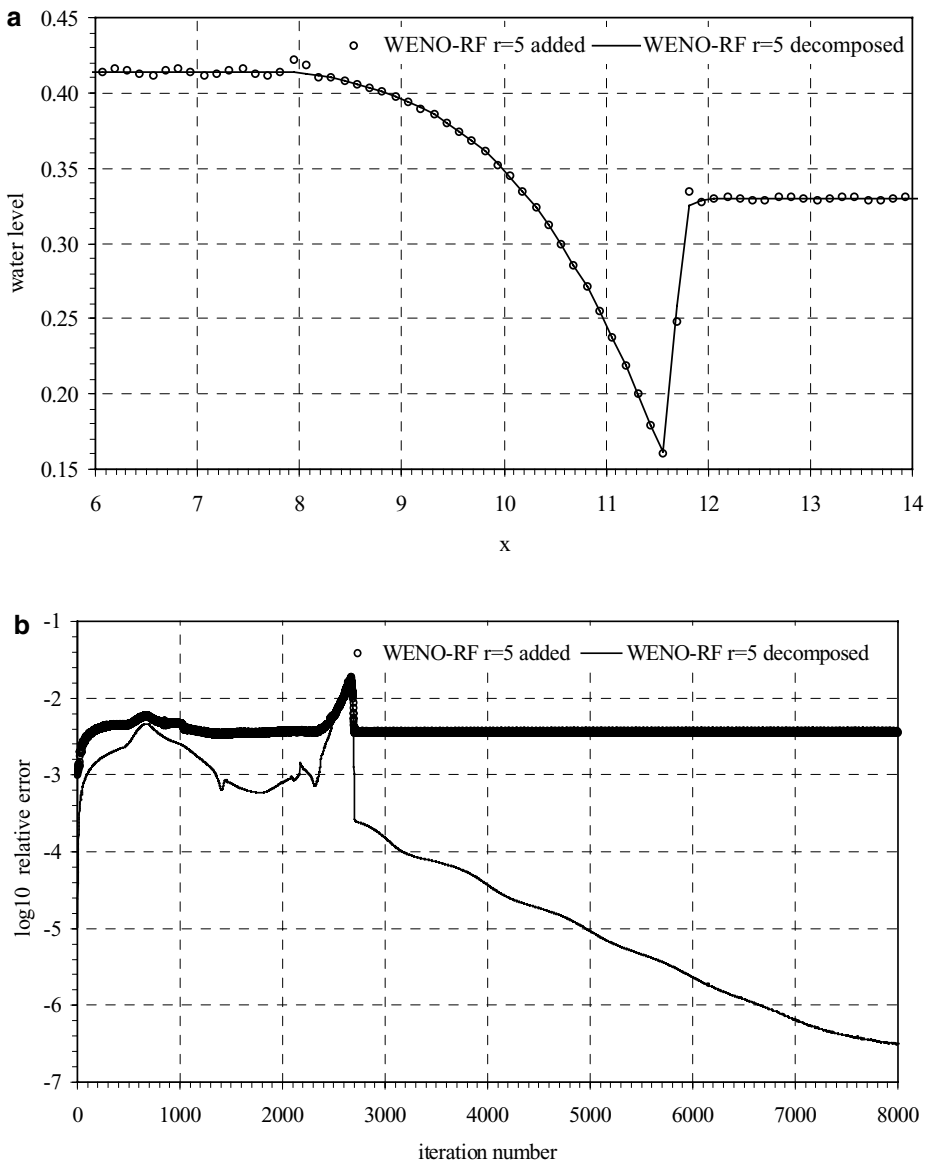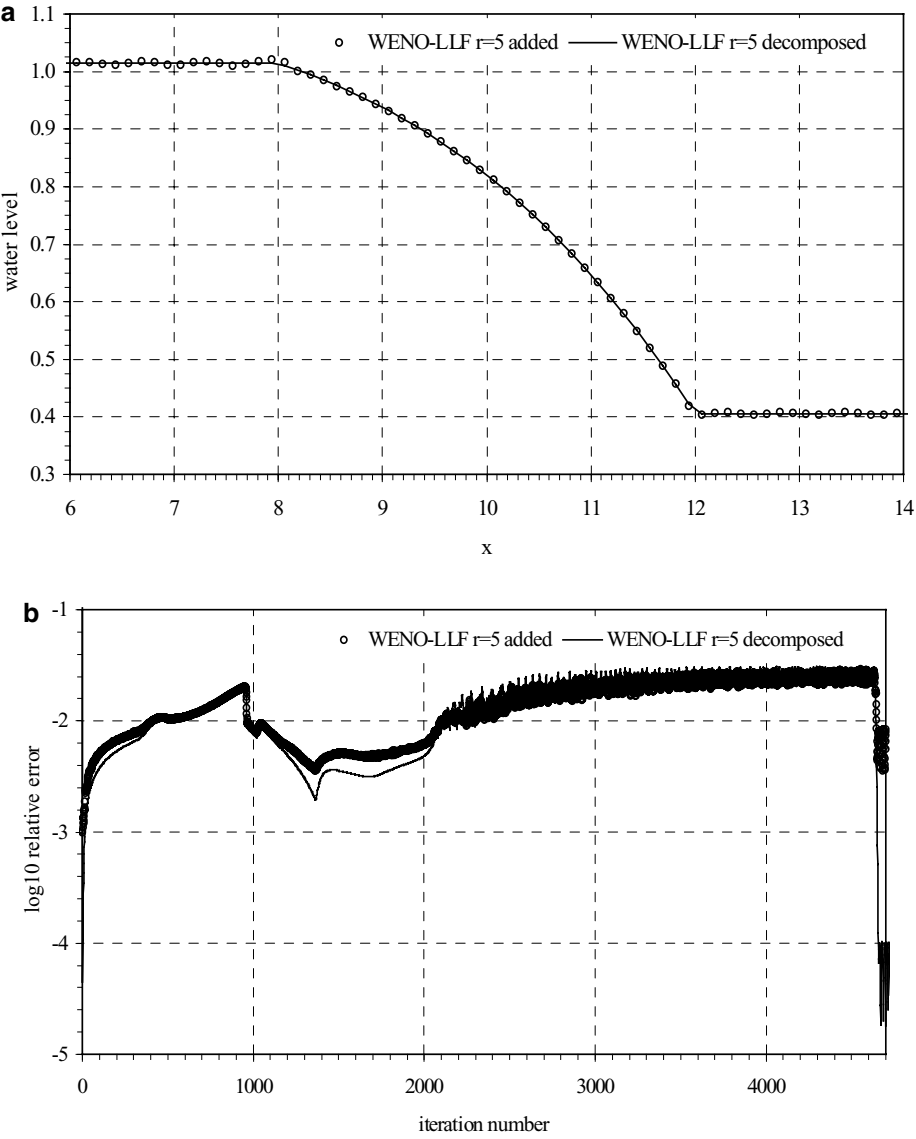
FIG. 5. Comparison of the WENO-RF, $r = 5$, schemes for the hydraulic jump over a bump (test problem (a) in Section 6.3). (a) Detail over the bump, water level at $t = 200$ s; (b) convergency history.

and with the inclusion of that singular error the difference between the schemes would be lost. In both cases we can observe the improvement introduced with the source term decomposition. The oscillations that occur downstream from the jump are smaller when WENO schemes of lower order are applied. Also, some very small oscillations appear for higher order decomposed WENO schemes that are not present in lower order cases. In our opinion this might be connected with the similar deteriorations in the order of accuracy for higher order cases, as we experimentally established in the test problem in Section 6.1, and possibly connected with accumulation of the round-off error. Further study is needed.

TABLE III

The L^∞ Error in the Unit Discharge for the Steady Flow over a Bump (Test Problem in Section 6.3)

Method	L^∞ error for 6.3.a	L^∞ error for 6.3.b
Q-scheme	4.7×10^{-5}	5.3×10^{-4}
Flux limited scheme	2.68×10^{-4}	4.0×10^{-5}
WENO-RF, $r = 5$, added	1.015×10^{-2}	1.72×10^{-2}
WENO-RF, $r = 5$, decomposed	4.0×10^{-6}	4.6×10^{-6}
WENO-LLF, $r = 5$, added	1.053×10^{-2}	1.556×10^{-2}
WENO-LLF, $r = 5$, decomposed	8.0×10^{-6}	1.1×10^{-4}

FIG. 6. Comparison of the WENO-LLF, $r = 5$, schemes for the steady transcritical flow over a bump (test problem (b) in Section 6.3). (a) Detail over the bump, water level at $t = 200$ s; (b) convergency history.

6.4. *A Problem Discussed by LeVeque*

This test problem, proposed by LeVeque [16], is a nonstationary f ow, with actually two dam breaks that propagate in opposite directions, and in addition, while the upstream moving front passes over a horizontal riverbed, the downstream moving front propagates over a bump. The bed slope is continuous. So with this problem we test scheme performance on a rapidly varying f ow over a smooth bed.

The bed is given with

$$z(x) = \begin{cases} 0.25(\cos(10\pi(x-0.5))+1) & \text{if } 1.4 \le x \le 1.6 \\ 0 & \text{otherwise,} \end{cases} \tag{65}$$

and $M = 0$. The initial conditions are given with

$$v(x, 0) = 0 \quad \text{and} \quad h(x, 0) = \begin{cases} 1. + \Delta h - z(x) & \text{if } 1.1 \le x \le 1.2 \\ 1. - z(x) & \text{otherwise,} \end{cases} \tag{66}$$

where Δh is the height of the pulse. We test two cases:

(a) big pulse, i.e., $\Delta h = 0.2$ (initial condition in Fig. 7), and
(b) small pulse, i.e., $\Delta h = 0.001$.

Originally, LeVeque solved this test problem with $g = 1 \text{ m/s}^2$ while we, as in all test problems in this section, use $g = 9.81 \text{ m/s}^2$. We preformed all the computations using space step $\Delta x = 0.001 \text{ m}$ and the CFL coeff cient $c_{cfl} = 0.5$. In Figs. 8 and 9 we present results obtained with ENO-RF scheme with a two-step Runge–Kutta time integration and with $r = 1$.
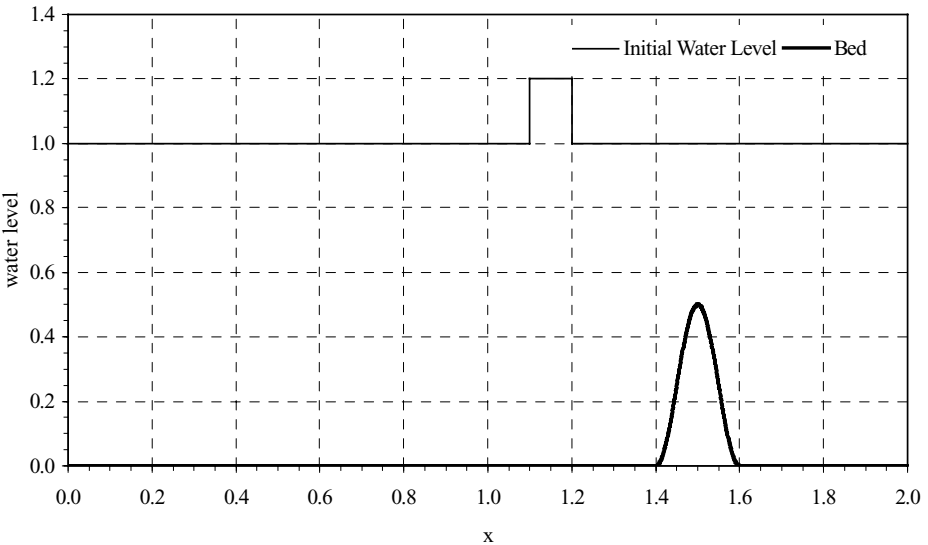

FIG. 7. The initial water level and bed for the problem discussed by LeVeque (test problem (a) in Section 6.4).
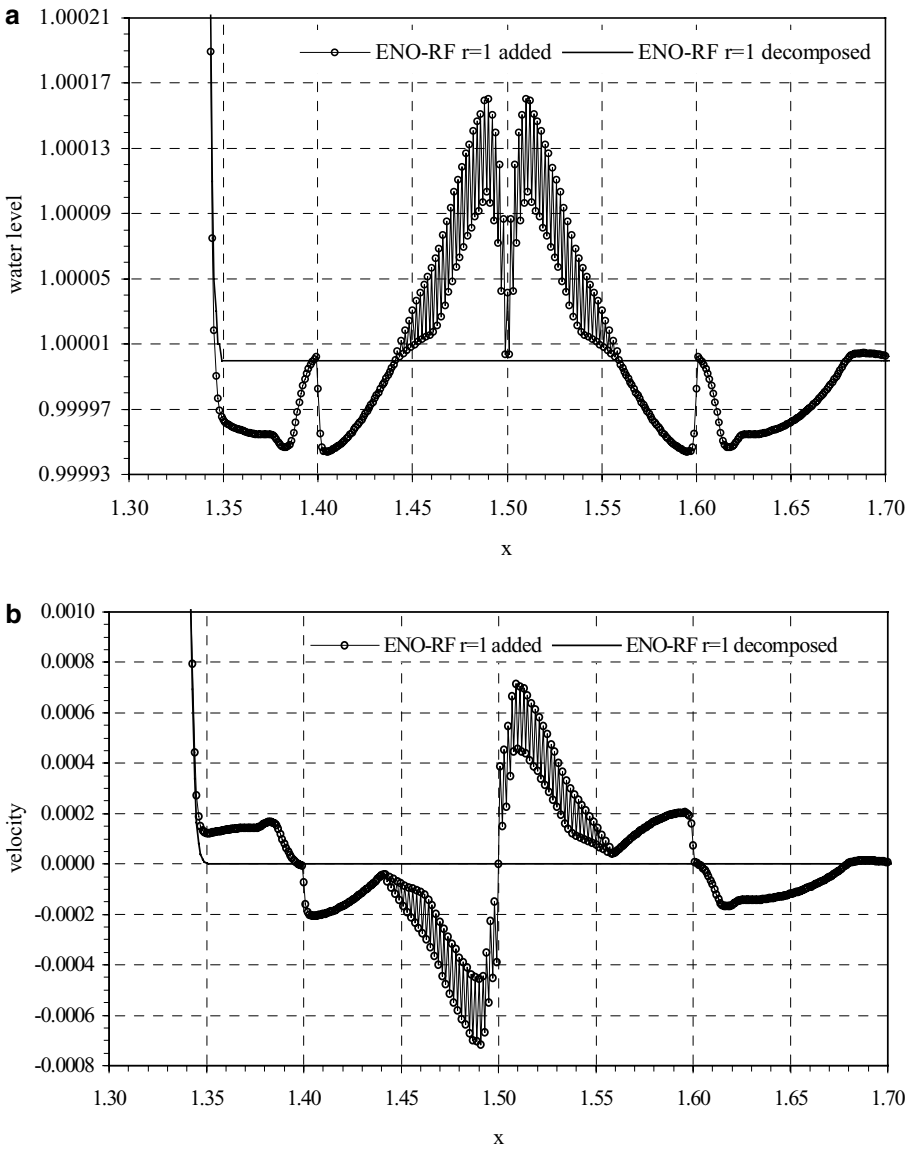
a

b

FIG. 8. Comparison of the ENO-RF, $r = 1$, schemes for the problem discussed by LeVeque with big pulse (test problem (a) in Section 6.4). Detail over the bump: (a) water level at $t = 0.04$ s; (b) velocity at $t = 0.04$ s.

In Fig. 8 we show results for the big pulse and the water level and velocity in the part of the domain over the bump at time $t = 0.04$ s. We chose this particular moment because the downstream-traveling water pulse had not yet reached the bump. So the oscillations that we observe in the ENO schemes with the source term added are only due to the inability of that scheme to preserve the quiescent f ow. Since the L^∞ error is around 10^{-5} for the water level and around 10^{-4} for the velocity the difference between the ENO schemes with the source term added and ENO schemes with the source term decomposed is not visible after the big pulse passes over the bump. In fact since in this test problem the bed depth is artif cial and smoothly changing and the dominant effect is the pulse splitting and moving, even the ENO schemes with source term added give, on the global scale,

satisfying results. In [10] we can see results for the same test problem tested with several other schemes, and observe that for some other schemes the nondecomposed version does not work as well. So we can conclude that if the scheme is accurate enough, the bed level is smooth, and the f ow is rapidly varying, the source decomposition might not be that important. In [16] LeVeque gives a similar observation. However, this is only due to the fact that in these cases the error due to the source term pointwise evaluation is much smaller then the f ow perturbation and it cannot be registered. Actually, in case (b) of the small pulse the same perturbation structure caused by the numerical error in the evaluation of the source term can be clearly observed even after the pulse passes over the bump (Fig. 9).
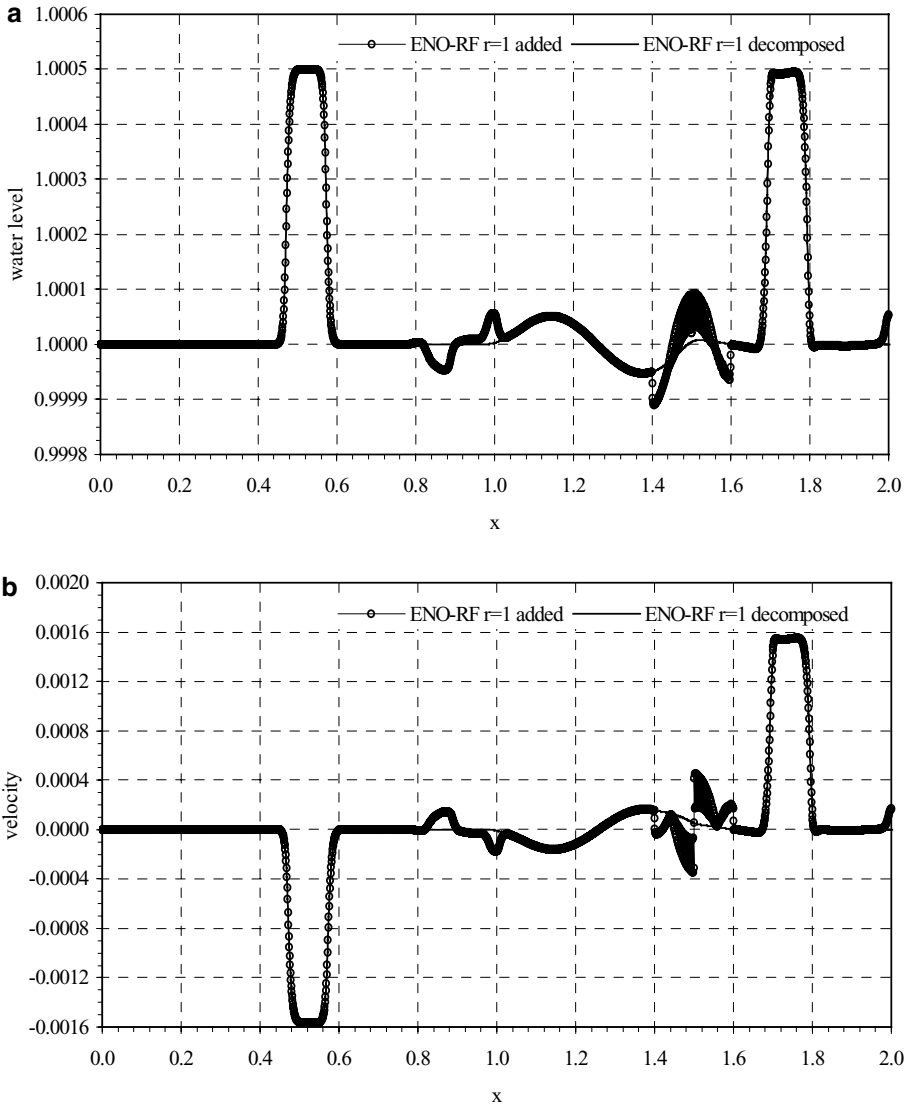

FIG. 9. Comparison of the ENO-RF, $r = 1$, schemes for the problem discussed by LeVeque with small pulse (test problem (b) in Section 6.4). Detail over the bump: (a) water level at $t = 0.2$ s; (b) velocity at $t = 0.2$ s.

6.5. *The Dam Break over the Rectangular Bump*

The purpose of the last test problem is to test the new approach in the case of a rapidly varying f ow over discontinuous bed slope. The bed level is given with

$$z(x) = \begin{cases} 8 & \text{if } |x - 1500/2| \leq 1500/8 \\ 0 & \text{otherwise,} \end{cases} \tag{67}$$
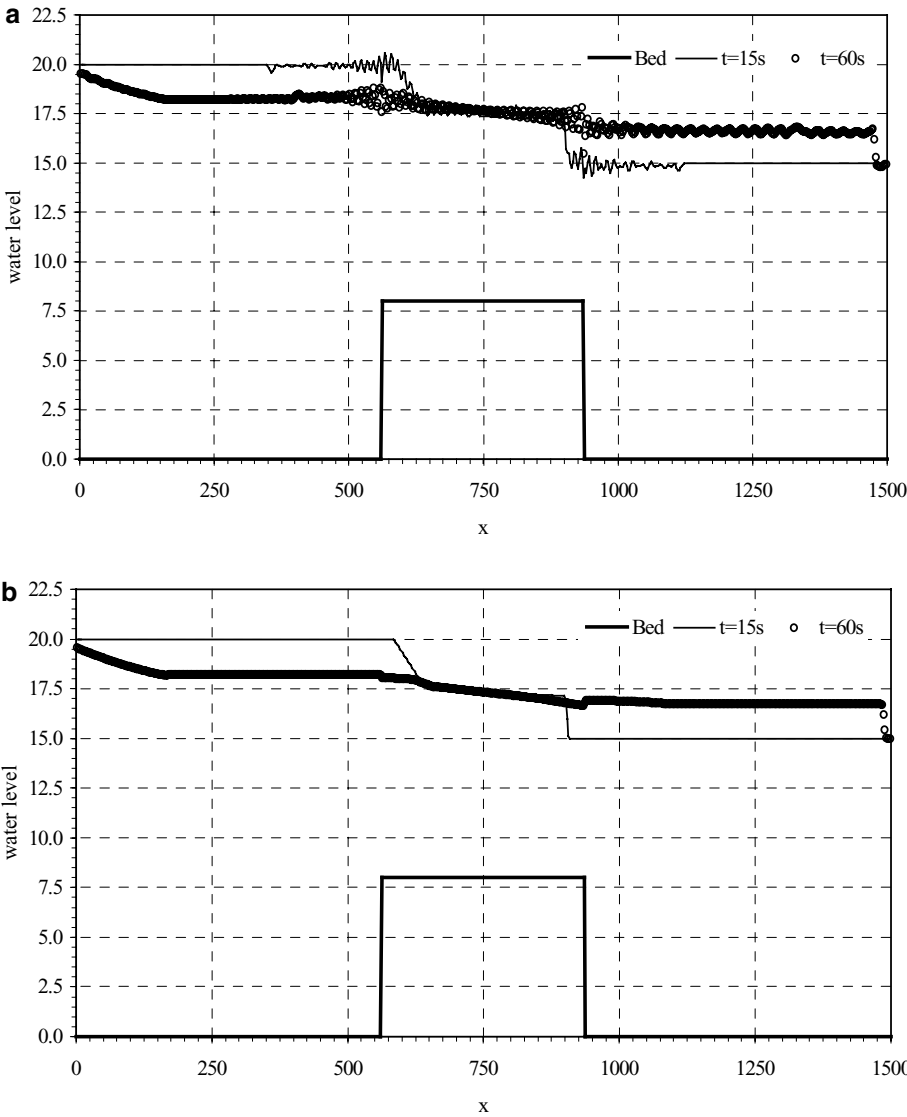

FIG. 10. Water level for the dam break over the rectangular bump (test problem in Section 6.5). (a) WENO-LLF, $r = 5$, scheme with source term added; (b) WENO-LLF, $r = 5$, scheme with source term decomposed; (c) the f ux limited scheme with source term decomposed [8].
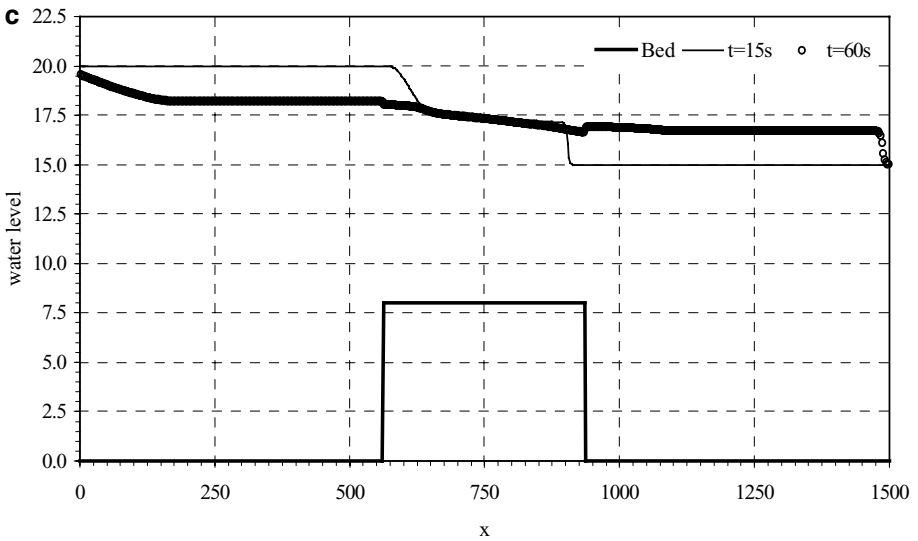
FIG. 10—*Continued*

the friction is set to $M = 0.1$, and the initial conditions are

$$H(x, 0) = \begin{cases} 20 & \text{if } x \leq 750 \\ 15 & \text{otherwise} \end{cases} \quad \text{and} \quad v(x, 0) = 0 \, \text{m/s}. \tag{68}$$

So, it is a dam break problem over a bed with a rectangular bump exactly under the dam. In fact this problem is a mixture of test problems in other references. We took the riverbed from [25] and the idea of observing a dam break on a variable-depth riverbed from [10].

All the computations are performed with the space step $\Delta x = 2.5$ m and the CFL coefficient $c_{cfl} = 0.6$. Results are given in Fig. 10. The used WENO-LLF scheme is with $r = 5$ and a three-step Runge–Kutta time integration. Comparison between Figs. 10a and 10b clearly illustrates the importance of the introduced decomposition in the WENO schemes even for rapidly varying f ows over a nonsmooth bed. The nondecomposed version gives very poor results since the magnitude of the numerical error caused by the source term pointwise evaluation is the same as that of the perturbation in f ow caused by the dam break. This is a consequence of the discontinuous bed slope, which is typical in natural watercourses. Comparison between Figs. 10b and 10c gives some insight into these and other schemes; in particular it shows that the new WENO schemes are more accurate and shock capturing then the second-order f ux limited scheme with source term decomposed [8, 9]. This is inherited from the original ENO and WENO schemes.

7. CONCLUDING REMARKS

The new ENO and WENO schemes with the source term decomposed that we propose in this paper can be viewed as a natural way to apply the ENO or WENO reconstruction to the entire right side in (2), i.e., to (3) and not only to the f ux term, in the case of conservation laws with geometrical source terms. The resulting schemes are high resolution, even if with an order of accuracy apparently reduced in comparison to original ENO and WENO

schemes for homogeneous systems (test problem in Section 6.1). Also they present better shock-capturing property when compared with some other upwind schemes (test problem in Section 6.5). Finally, when applied to the shallow water equations, the new schemes verify the exact conservation property [2, 3].

REFERENCES

1. D. S. Balsara and C.-W. Shu, Monotonicity preserving weighted essentially nonoscillatory schemes with increasingly high order of accuracy, *J. Comput. Phys.* **160**, 405 (2000), doi:10.1006/jcph.2000.6443.

2. A. Bermùdez, A. Dervieux, J. A. Désidéri, and M. E. Vázquez, Upwind schemes for the two-dimensional shallow water equations with variable depth using unstructured meshes, *Comput. Methods Appl. Mech. Eng.* **155**, 49 (1998).

3. A. Bermùdez and M. E. Vázquez, Upwind methods for hyperbolic conservation laws with source terms, *Comput. Fluids* **23**(8), 1049 (1994).

4. R. Botchorishvilli, B. Pertham, and A. Vasseur, *Equilibrium Schemes for Scalar Conservation Laws with Stiff Sources*, Report DMA 00-16 (Département de mathématique et applications (DMA), École normale supérieure, Paris, 2000).

5. A. Chinnayya and A.-Y. LeRoux, *A New General Riemann Solver for the Shallow Water Equations, with Friction and Topography* (University Bordeaux I, Department of Mathematics, 1999).

6. J. M. Greenberg and A.-Y. LeRoux, A well-balanced scheme for the numerical processing of source terms in hyperbolic equations, *SIAM J. Numer. Anal.* **33**, 1 (1996).

7. A. Harten and S. Osher, Uniformly high-order accurate non-oscillatory schemes, I, *SIAM J. Numer. Anal.* **24**, 279 (1987).

8. A. Harten, B. Engquist, S. Osher, and S. R. Chakravarthy, Uniformly high-order accurate non-oscillatory schemes, III, *J. Comput. Phys.* **71**, 231 (1987).

9. M. E. Hubbard and P. Garcia-Navarro, Flux difference splitting and the balancing of source terms and f ux gradients, *J. Comput. Phys.* **165**, 89 (2000), doi:10.1006/jcph.2000.6603.

10. J. Hudson, *Numerical Techniques for the Shallow Water Equations*, Numerical Analysis Report (University of Reading, Department of Mathematics, 1999).

11. P. Jenny and B. Müller, Rankine–Hugoniot–Riemann solver considering source terms and multidimensional effects, *J. Comput. Phys.* **145**, 575 (1998), doi:10.1006/jcph.1998.6037.

12. G. Jiang and C.-W. Shu, Eff cient implementation of weighted ENO schemes, *J. Comput. Phys.* **126**, 202 (1996).

13. G. Jiang and C. Wu, A high-order WENO f nite difference scheme for the equations of ideal magnetohydrodynamics, *J. Comput. Phys.* **150**, 561 (1999), doi:10.1006/jcph.1999.6207.

14. S. Jin, *A Steady-State Capturing Method for Hyperbolic Systems with Geometrical Source Terms* (University of Wisconsin, Department of Mathematics, 2000).

15. S. Jin and Z. Xin, The relaxation schemes for systems of conservation laws in arbitrary space dimensions, *Commun. Pure Appl. Math.* **48**, 235 (1995).

16. R. J. LeVeque, *Balancing Source Terms and Flux Gradients in High-Resolution Godunov Methods: The Quasi-Steady Wave Propagation Algorithm*, Numerical Analysis Report (Department of Applied Mathematics and Department of Mathematics, University of Washington, 1998).

17. R. J. LeVeque and D. S. Bale, Wave propagation methods for conservation laws with source terms, in *Proceedings of the 7th International Conference on Hyperbolic Problems, Zürich*, edited by R. Jeltsch and M. Fey (Birkhauser, Boston, 1999).

18. V. Martinez and A. Marquina, *Computation of Traveling Wave Solutions of Scalar Conservation Laws with a Stiff Source Term*, GrAN Report 99-06 (University of Valencia, Department of Mathematics, 1999).

19. P. Montarnal and C.-W. Shu, Real gas computation using an energy relaxation method and high-order WENO schemes, *J. Comput. Phys.* **148**, 59 (1999), doi:10.1006/jcph.1998.6105.

20. P. L. Roe, Upwinded difference schemes for hyperbolic conservation laws with source terms, in *Proceedings of the Conference on Hyperbolic Problems*, edited by A. S. Carasso, P. A. Raviart, and J. P. Serre (Springer-Verlag, Berlin/New York, 1986), p. 41.

21. C.-W. Shu and S. Osher, Eff cient implementation of essentially non-oscillatory shock-capturing schemes, *J. Comput. Phys.* **77**, 439 (1988).

22. C.-W. Shu and S. Osher, Eff cient implementation of essentially non-oscillatory shock-capturing schemes, II, *J. Comput. Phys.* **83**, 32 (1989).

23. C.-W. Shu, Essentially non-oscillatory and weighted essentially non-oscillatory shock-capturing schemes for hyperbolic conservation laws, in *Advanced Numerical Approximation of Nonlinear Hyperbolic Equations*, edited by B. Cockburn, C. Johnson, C.-W. Shu, and E. Tadmor, Lecture Notes in Mathematics (Springer-Verlag, Berlin/New York, 1998), Vol. 1697, p. 325.

24. P. K. Smolarkiewicz and L. G. Margolin, MPDATA: A f nite-difference solver for geophysical f ows, *J. Comput. Phys.* **140**, 459 (1998), doi:10.1006/jcph.1998.5901.

25. M. E. Vázquez-Cendón, Improved treatment of source terms in upwind schemes for the shallow water equations in channels with irregular geometry, *J. Comput. Phys.* **148**, 499 (1999), doi:10.1006/jcph.1998.6127.

26. J. G. Zhou, D. M. Causon, C. G. Mingham, and D. M. Ingram, The surface gradient method for the treatment of source terms in the shallow-water equations, *J. Comput. Phys.* **168**, 1 (2001), doi:10.1006/jcph.2000.6670.